ISSN 1070-3284, Russian Journal of Coordination Chemistry, 2022, Vol. 48, No. 2, pp. 118–126. © Pleiades Publishing, Ltd., 2022.

Crystal Structures and Fluorescent Properties of Two Distinct 2D Ag(I)/Cd(II) Coordination Polymers Based on Isonicotinic Acid Derivative and Dipyridyl Coligand

L. Y. Xin[a], Y. P. Li[a], F. Y. Ju[b], X. L. Li[a], and G. Z. Liu[a, *]

[a] *College of Chemistry and Chemical Engineering, and Henan Key Laboratory of Fuction-Oriented Porous Materials, Luoyang Normal University, Luoyang, 471934 P.R. China*

[b] *School of Food and Drug, Luoyang Normal University, Luoyang Normal University, Luoyang, 471934 P.R. China*

**e-mail: gzliuly@126.com*

Received July 6, 2021; revised August 14, 2021; accepted August 15, 2021

Abstract—Two novel coordination polymers obtained by hydrothermal reaction of Ag(I) nitrate and Cd(II) acetate salts with 3,5-dichloroisonicotinic acid and 1,3-bis(4-pyridyl)propane flexible ligand have been synthesized and characterized by single crystal X-ray diffraction (CIF files nos. 2082469 (**I**) and 2082471 (**II**)), elemental analyses, thermogravimetric analyses, powder X-ray diffractions and fluorescent spectra, formulated as $\{[Ag(Bpp)](Dcia)\}_n$ (**I**) and $[Cd(Dcia)_2(Bpp)_2]_n$ (**II**) (HDcia = 3,5-dichloroisonicotinic acid, Bpp = 1,3-bis(4-pyridyl)propane). The single-crystal X-ray diffractions reveal that two complexes show different 2D $\{6^3\}$ *hcb* topological nets and (4,4) grid layers displaying remarked structural sensitivity to metal cation. Among them, complex **I** displays 2D unusual cationic layer developed by T-shaped Bpp-bridging Ag–Ag building units. Complex **II** exhibits 2D grid layer jointed by Dcia ligand with dangling Bpp ligand, which further interlinked into 3D supramolecular architecture by π–π interactions. In addition, luminescent properties of both complexes are also systematically investigated.

Keywords: coordination polymer, hydrothermal reaction, 3,5-dichloroisonicotinic acid, luminescent properties

DOI: 10.1134/S1070328422020063

INTRODUCTION

The metal-organic coordination polymers (CPs), known as complexes combining the features of inorganic metal ions and organic ligands, have been becoming one of the most rapidly developing fields in chemical and material science not only because of their highly diversified topologies, but also due to their potential applications in many areas, such as sensing [1, 2], conductivity [3, 4], magnetism [5, 6], catalysis [7, 8], luminescence [9, 10] and so on. At present, many multitopic organic ligands have been widely employed to prepare such crystalline materials either O-donor ligands (such as 1,2-benzenebicarboxylate [11–13], 1,3,5-benzenetricarboxylate [14–16] and 1,2,4,5-benzenetetracarboxylate [17–19]), or N-donor ligands (such as 4,4'-bipyridine [20–22], 1,2-bis(4-pyridyl)ethylene [23–25] and 1,3-bis(4-pyridyl)propane [26–28]) as linkers. Notably, isonicotinic acid as polydentate bifunctional ligand has been widely used due to the ingenious combination of carboxyl group and a pyridyl ring [29–31]. On the one hand, the carboxyl group may be conductive to the formation of discrete metal center and infinite building blocks by M–COO–M linkages. On the other hand, pyridyl group may have the ability to link these units to an intricate extended network.

As a novel isonicotinic acid derivative, the 3,5-dichloroisonicotinic acid (HDcia) is also ideal bifunctional connector in the exploration for CPs. Though as a good bifunctional ligand, HDcia remains largely unexplored, and only few CPs have been reported. So far, we know of only five known structures that have been reported [32–36]. In this regard, we hope to reveal more structural factors of the HDcia for dominating the self-assemblies of CPs, and this will provide more useful information of the substituent effect. Furthermore, the addition of neutral dipyridyl coligands can provide much more complicated and fascinating structures in view of their cooperative coordination. As a result, the insertion of additional ligands in the synthesis media can have a crucial effect on the dimensionality of the resulting network.

With these considerations in mind, we choose the bifunctional 3,5-dichloroisonicotinic acid (HDcia) as bridging ligand, and flexible 1,3-bis(4-pyridyl)propane (Bpp**)** as the coligand in this synthesis system. In this work, systematic studies have been carried out in our laboratory by the reaction of Ag(I) nitrate and

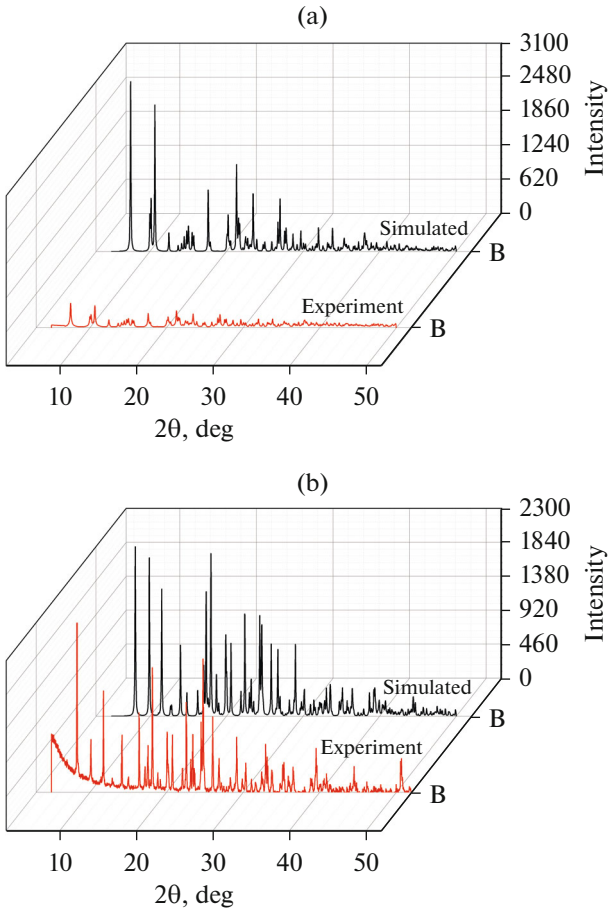

Fig. 1. PXRD pattern for complexes **I** (a) and **II** (b).

Cd(II) acetate with the HDcia and Bpp flexible ligand producing two coordination polymers with the range of structure from 2D $\{6^3\}$ *hcb* topology layer developed by T-typed building units, $\{[Ag(Bpp)](Dcia)\}_n$ (**I**) to 2D grid Cd(II) carboxylate layer, $[Cd(Dcia)_2(Bpp)_2]_n$ (**II**). The details of their synthesis conditions, coordination structures and luminescent properties are reported below.

EXPERIMENTAL

Materials and physical measurements. All reagents were commercially purchased and used directly without further purification. Elemental analyses for C, H, and N were performed on a Flash EA 2000 elemental analyzer. The powder X-ray diffraction (PXRD) patterns of the products were recorded with a Bruker AXS D8 Advance diffractometer using monochromatic CuK_α radiation (λ = 1.5418 Å; generator current: 40 mA; generator voltage: 40 kV; scanning scope: 2θ = 5°–50°). The thermogravimetric analyses (TGA) were carried out on a SII EXStar6000 TG/DTA6300 analyzer with a heating rate of 10°C min^{-1} under N_2 atmosphere. Luminescence spectra of the solid samples were performed at the room temperature on a Hitachi F-4500 spectrophotometer with xenon arc lamp as the light source.

Synthesis of compound $\{[Ag(Bpp)](Dcia)\}_n$ (I) was carried out by the solvothermal methods. A mixture of HDcia (0.1 mmol, 19.2 mg), Bpp (0.1 mmol, 19.8 mg), $AgNO_3$ (0.1 mmol, 17.0 mg) and H_2O (6.0 mL) was placed in a 23 mL Teflon liner stainless steel reactor. The vessel was heated to 393 K for 4 days, then cooled slowly to the room temperature. Colourless crystals were obtained, and further crystals were filtered off, washed with mother liquid, and dried under ambient conditions. The yield was 39% (based on HDcia ligand). The PXRD patterns of the bulk products are in well agreement with the simulated patterns based on the structure solutions (Fig. 1a).

For $C_{19}H_{16}N_3O_2Cl_2Ag$			
Anal. calcd., %:	C 45.91	H 3.24	N 8.45
Found, %:	C 45.88	H 3.42	N 8.49

Synthesis of $[Cd(Dcia)_2(Bpp)_2]_n$ (II) was carried out by using similar method as complex **I**, except that $AgNO_3$ was replaced by $Cd(OAc)_2{\cdot}2H_2O$ (0.1 mmol, 26.7 mg). Colourless crystals were obtained. The yield was 42% (based on HDcia ligand). The PXRD patterns of the bulk products are in well agreement with the simulated patterns based on the structure solutions (Fig. 1b).

For $C_{38}H_{32}N_6O_4Cl_4Cd$			
Anal. calcd., %:	C, 51.23	H, 3.62	N 9.43
Found, %:	C, 51.28	H, 3.71	N 9.40

X-ray crystallography. Single-crystal X-ray diffraction data for complexes **I** and **II** were recorded at room temperature on a Bruker SMART APEX II CCD diffractometer equipped with graphite-monochromated MoK_α radiation (λ = 0.71073 Å). Using Olex2 [37], the structure was solved with the Olex2.solve [38] structure solution program using Charge Flipping and refined with the ShelXL [39] refinement package using Least Squares minimisation. Semi-empirical absorption corrections were applied using SADABS. The structures were solved using direct method and refined by full-matrix least-squares on F^2. All non-hydrogen atoms were refined anisotropically, and the hydrogen atoms were placed in calculated positions and refined isotropically with a riding model except for those bound to water molecules, which were initially located in a difference Fourier map and included in the final refinement by use of geometrical restraints with the O–H distances being fixed at 0.85 Å and U_{iso}(H) equivalent to 1.5 times of U_{eq}(O). Crystal data and experimental details for compounds **I** and **II** are contained in Table 1. Selected bond distances/angles

Table 1. Crystallographic data and structure refinements for complexes **I** and **II**

Parameter	Value	
	I	**II**
Empirical formula	$C_{19}H_{16}N_3O_2Cl_2Ag$	$C_{38}H_{32}N_6O_4Cl_4Cd$
Formula weight	497.12	890.9
Crystal system	Monoclinic	Monoclinic
Space group	$P2_1/n$	$P2_1/c$
a, Å	9.4393(6)	11.4333(6)
b, Å	8.8570(5)	11.5552(5)
c, Å	23.5721(11)	14.6094(6)
α, deg	90	90
β, deg	91.311(5)	107.579(5)
γ, deg	90	90
Volume, Å^3	1970.2(2)	1839.97(15)
Crystal size, mm	0.32 × 0.28 × 0.22	0.36 × 0.31 × 0.28
Z	4	2
ρ_{calcd}, g cm^{-3}	1.676	1.551
μ, mm^{-1}	1.313	0.932
F(000)	992.0	837.0
θ Range, deg	3.28–25.5	3.42–25.49
Reflections collected	10754	9968
Independent reflections (R_{int})	3630 (0.0286)	3384 (0.0277)
Parameters	3630/0/244	3384/0/241
Goodness-of-fit	1.020	1.056
Final R indices ($I > 2\sigma(I)$)	$R_1 = 0.0357$, $wR_2 = 0.0608$	$R_1 = 0.0263$, $wR_2 = 0.0571$
R indices (all data)	$R_1 = 0.0515$, $wR_2 = 0.0648$	$R_1 = 0.0324$, $wR_2 = 0.0601$
Largest diff. peak and hole, e Å^{-3}	0.41/–0.41	0.32/–0.28

and hydrogen bonds are listed in Table 2 and Table 3, respectively.

Crystallographic data for the structural analysis have been deposited with the Cambridge Crystallographic Data Center (CCDC nos. 2082469 (**I**) and 2082471 (**II**); deposit@ccdc.cam.ac.uk or http://www.ccdc.cam.ac.uk).

RESULTS AND DISCUSSION

Complex **I** exhibits a unusual 2D cationic layer with 3-connected {6^3} *hcb* topology. As revealed by single-crystal X-ray diffraction, the asymmetric unit of complex **I** contains one Ag(I) cation, one Bpp ligand and uncoordinated Dcia anion, as shown in Fig. 2a. Each silver(I) is linked to two nitrogens of different but symmetry-equivalent Bpp molecules in a nearly linear coordination (the Ag–N bond lengths are 2.180(2) and 2.183(2) Å, ∠NAg(2)N(3A) 160.75(9)°, which are in the normal range (Table 2) [28, 40]) to form extended chains. Adjacent chains are cross-linked in an almost perpendicular fashion (Ag(1)–Ag(1A) bond length is 3.1130(6) Å, ∠N(2)Ag(1)Ag(1A) 94.44(6)°, ∠N(3B)Ag(1)Ag(1A) 97.97(7)°, which are in the normal range (Table 2) [41, 42]) by Ag–Ag bonds leading to a 2D cationic layer as represented in Fig. 2b.

From a topological perspective, complex **I** can be described as a 3-connected net with {6^3} *hcb* topology (Fig. 2c), in which each Ag(I) metal center as 3-connected node is linked to another Ag(I) center and two Bpp ligands as bridges. Adjacent cationic layers depend on the H-bonding interaction between the donor H atoms of benzene ring in Bpp ligands and the oxygen atoms of carboxylate ionic groups (C(11)–H(11)...O(1)$^{\#1}$ and C(12)–H(12)...O(2)$^{\#2}$ (Table 3) to develop into two-dimensional thick layer, as shown in the Fig. 2d. The adjacent 2D layers stack in a slightly off-set parallel fashion with the weak effect of van der Waals force to further extending 3D architecture.

Table 2. Selected bond lengths (Å) and angles (deg) for compounds **I** and **II***

Bond	*d*, Å	Bond	*d*, Å
		I	
Ag(1)–N(2)	2.180(2)	Ag(1)–N(3)$^{\#2}$	2.183(2)
Ag(1)–Ag(1)$^{\#1}$	3.1130(6)		
		II	
Cd(1)–O(1)	2.2888(14)	Cd(1)–O(1)$^{\#1}$	2.2889(14)
Cd(1)–N(1)$^{\#2}$	2.4262(17)	Cd(1)–N(1)$^{\#3}$	2.4262(17)
Cd(1)–N(2)	2.3002(18)	Cd(1)–N(2)$^{\#1}$	2.3002(18)
Angle	ω, deg	Angle	ω, deg
		I	
N(2)Ag(1)Ag(1)$^{\#1}$	94.44(6)	N(2)Ag(1)N(3)$^{\#2}$	160.75(9)
N(3)^{2}Ag(1)Ag(1)$^{\#1}$	97.97(7)		
		II	
O(1)Cd(1)O(1)$^{\#1}$	180.00(6)	O(1)$^{\#1}$Cd(1)N(1)$^{\#2}$	87.10(6)
O(1)Cd(1)N(1)$^{\#2}$	92.90(6)	O(1)$^{\#1}$Cd(1)N(1)$^{\#3}$	92.90(6)
O(1)Cd(1)N(1)$^{\#3}$	87.10(6)	O(1)Cd(1)N(2)	86.20(6)
O(1)$^{\#1}$Cd(1)N(2)	93.80(6)	O(1)Cd(1)N(2)$^{\#1}$	93.80(6)
O(1)$^{\#1}$Cd(1)N(2)$^{\#1}$	86.20(6)	N(1)$^{\#3}$Cd(1)N(1)$^{\#2}$	180.0
N(2)$^{\#1}$Cd(1)N(1)$^{\#3}$	88.11(6)	N(2)$^{\#1}$Cd(1)N(1)$^{\#2}$	91.89(6)
N(2)Cd(1)N(1)$^{\#3}$	91.89(6)	N(2)Cd(1)N(1)$^{\#2}$	88.11(6)
N(2)Cd(1)N(2)$^{\#1}$	180.0		

* Symmetry codes for compounds: $^{\#1}$ $-x, 1-y, 1-z$; $^{\#2}$ $-1/2+x, 1/2-y, -1/2+z$ (**I**); $^{\#1}$ $1-x, 2-y, 1-z$; $^{\#2}$ $1-x, 1/2+y, 1/2-z$; $^{\#3}$ $x, 3/2-y, 1/2+z$ (**II**).

Table 3. Geometric parameters of hydrogen bonds for compounds **I** and **II***

D–H···A	Distance, Å			
	D–H	H···A	D···A	∠DHA, deg
		I		
C(11)–H(11)...O(1)$^{\#1}$	0.93	2.56	3.336(4)	141.2
C(12)–H(12)...O(2)$^{\#2}$	0.93	2.55	3.250(4)	132.2
		II		
C(11)–H(11)...O(2)$^{\#1}$	0.95	2.55	3.466(3)	162.2

* Symmetry codes for compounds: $^{\#1}$ $1/2-x, -1/2+y, 3/2-z$ (**I**); $^{\#2}$ $1/2+x, 1/2-y, 1/2+z$; $^{\#1}$ $1-x, 2-y, 1-z$ (**II**).

Complex **II** exhibits a 2D layer structure developed by Dcia molecules, while Bpp molecules works as a terminal ligand with uncoordinated pyridine N atoms. The asymmetric unit of complex **I** consists of half a Cd(II) atom, one Dcia anion and one Bpp coligand (Fig. 3a). Each Cd center has an octahedrally coordinated geometry with the basal plane occupied by two oxygen atoms and two pyridyl N atoms from four Dcia ligands (among them, two Cd–O bond lengths are 2.2888(14) Å and two Cd–N bond lengths are 2.4262(17) Å), while two Bpp pyridyl N atoms occupy the apical sites (Cd–N 2.3002(18) Å) (Table 2), which are in the normal range [43, 44]. The $[CdO_2N_4]$ environment is best described as slightly distorted octahedron.

The carboxylate groups with monodentate coordinated modes and pyridyl N atoms of Dcia ligands bridge the adjacent Cd(II) atoms to yield a

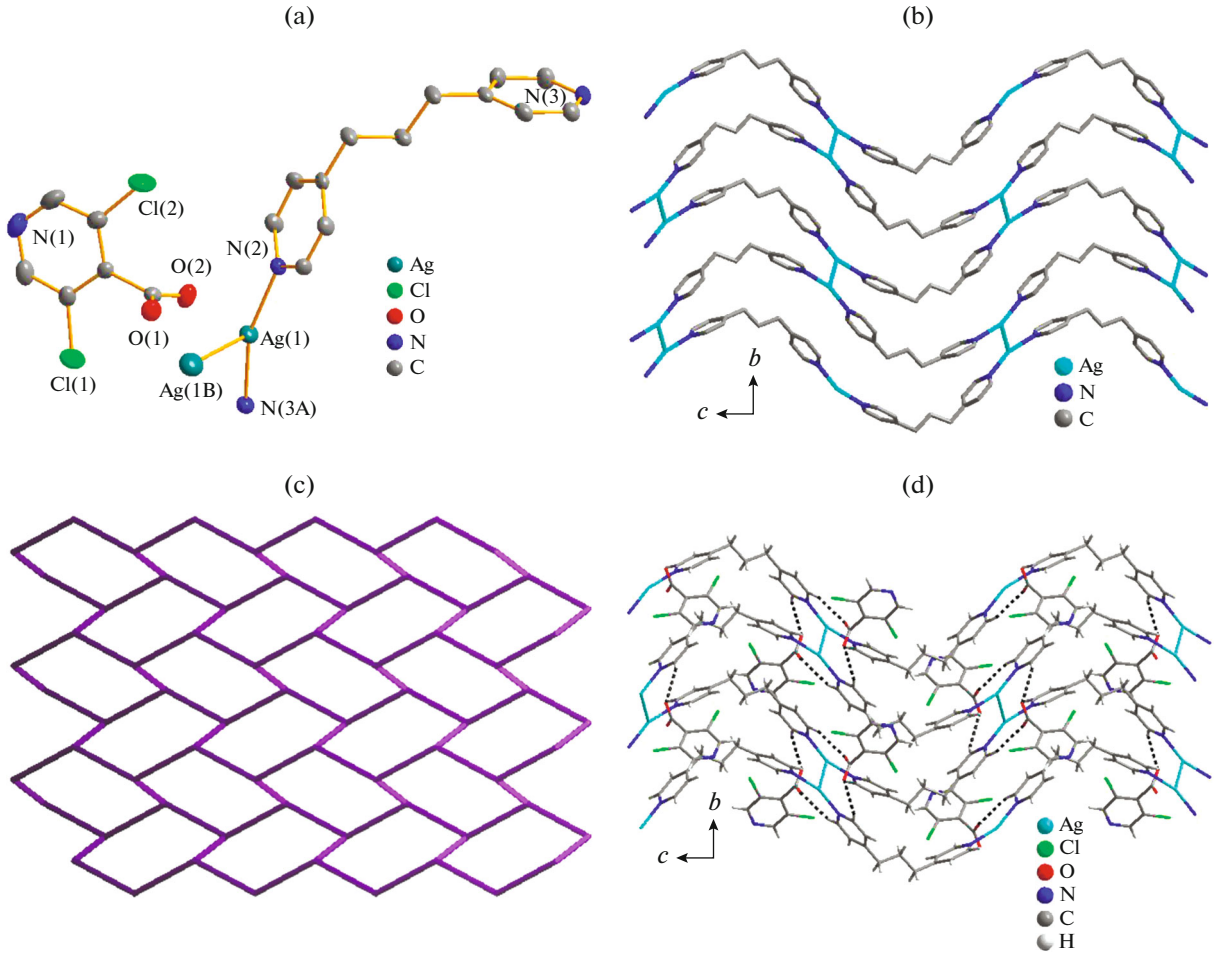

Fig. 2. View of the coordination environment of Ag(I) in **I** (symmetry codes: (A) $-0.5 + x$, $0.5 - y$, $-0.5 + z$; displacement ellipsoids are drawn at the 50% probability level and all hydrogen atoms of carbon atoms are omitted for clarity (a); view of 2D cationic layer developed by T-shaped building units (b); schematic representation of 3-connected $\{6^3\}$ ***hcb*** topology for **II** (c); view of 2D thick layer via H-bonded interactions (d).

$[Cd(Dcia)]_n$ (4,4) grid layer (Fig. 3b). Interestingly, the 2D layer involves two kinds of helical chains, where the right-handed and left-handed helical chains are in an alternate array by sharing the Dcia bridging ligand, as shown in Fig. 3c. The pitch of each helical chain is equivalent as the length of the *b*-axis, and the Bpp molecules as the terminal ligands like "fish" bite the Cd(II) center lying in the two sides of helical chain. So, the whole structure features 2D carboxylate layer developed by helical chains with dangling lateral arms. Weak π–π stacking interactions (the face-to-face distance is 3.935 Å) existing between both pyridyl rings of Bpp ligands from two adjacent layers, result in 3D supramolecular structure (Fig. 3d). π–π Stacking plays an important role in stabilizing the large structure. Here, by using the Atomistix ToolKit 2020 package [45, 46], we simulate the Bloch state of the compound **II** dependent on the density functional theory (DFT). Here, we adopted the approximation of the generalized gradient approximation (GGA) and the Perdew–Burke–Ernzerhof (PBE) functional [47]. Some Bloch states below the Fermi level are in Fig. 4. Figure 4b shows there is a π-like chemical bond in each ring. The A and B rings are stacked with a π–π bond. To investigate the inter-ring interaction, we calculated the binding energy by the following formula: $E_b = (E_t - E_A - E_B)/n$. E_t is the total energy of A and B when they are at the position as shown in Fig. 4a and E_A and E_B are the energy of isolated pyridine rings, and n is the total atom numbers. The calculated binding energy between A and B is only 3.1 meV/atom which is even smaller than that in graphene of 25 meV/atom [48]. Thus, it is a typical weak π–π stacking of intermolecular interactions. Besides, the inter-ring distance is 3.935 Å, which is larger than the van de Waas inter-layer distance of many two-dimensional materials. This also implies the inter-ring π–π interaction is very weak.

TGA for complexes **I** and **II** were performed on crystalline samples from room temperature to 900°C

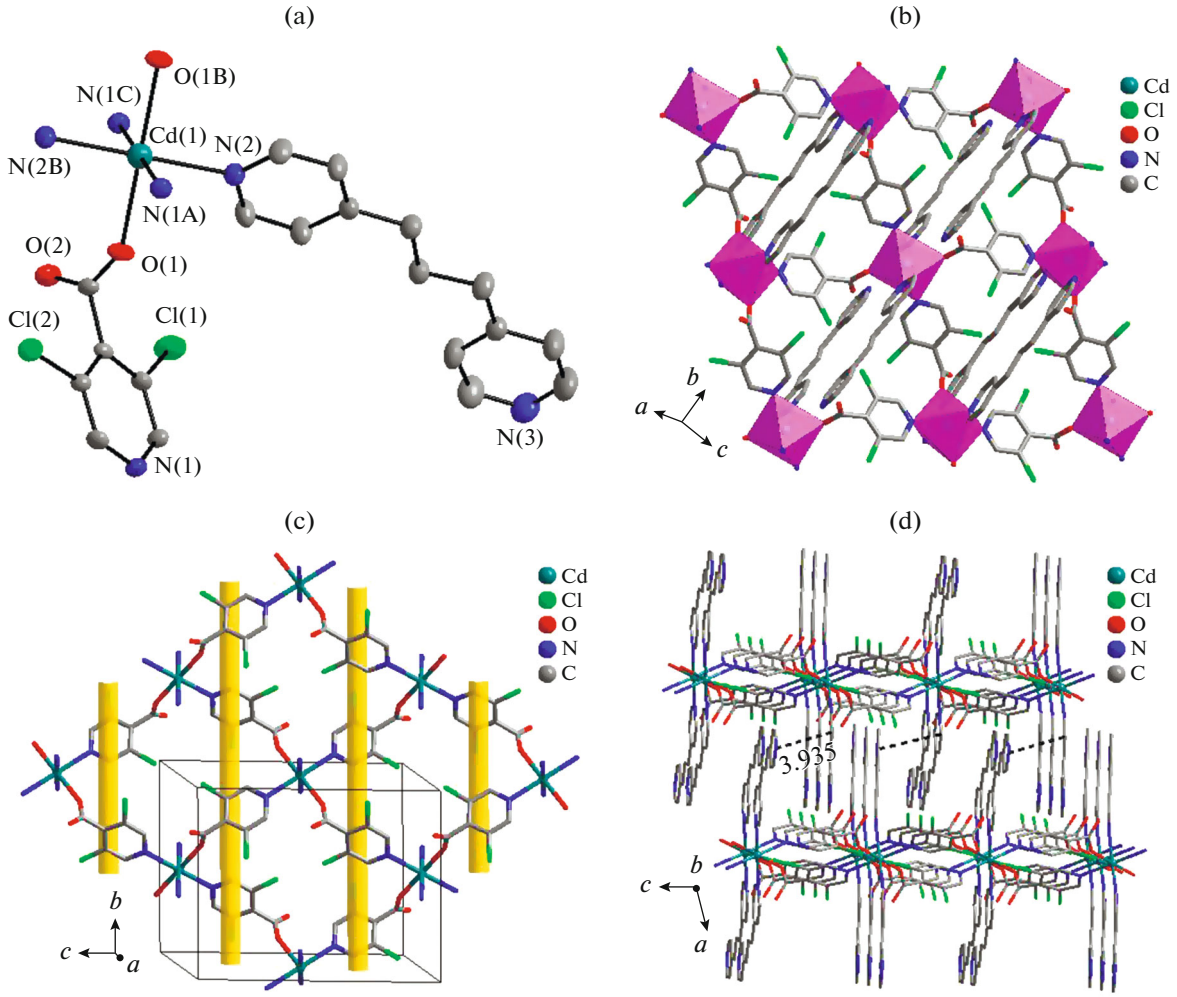

Fig. 3. View of the coordination environment of Cd(II) in **II** (symmetry codes: (A) $1-x$, $0.5+y$, $0.5-z$; (B) $1-x$, $2-y$, $1-z$; (C) x, $1.5-y$, $0.5+z$; displacement ellipsoids are drawn at the 50% probability level and all hydrogen atoms of carbon atoms are omitted for clarity) (a); view of a $[Cd(Dcia)]_n$ (4,4) grid layer (b); view of a 2D layer constructed via the left- and right-handed helical chains in **II** (c); view of 3D networks via π–π stacking interactions with face to face distance is 3.935 Å (d).

under a N_2 atmosphere to investigate their degradation behavior, as shown in Fig. 5. For compound **I**, no evident degradation process is observed before 192°C. It is proved the lamellar structure of compound **I** is stable before 190°C, and complete decomposition finishes at ~760°C. The observed final mass remnant of 23.99%, and mainly represented deposition of Ag phase which is agreed with the PXRD patterns of residuum (Fig. 6a). For complex **II**, the decomposition of the frameworks appears at ~200°C. After that, a series of consecutive weight losses until ~495°C corresponds to decomposition of organic ligands, and the remnant is 13.50%, and mainly represented CdO phase which is agreed with the PXRD patterns of residuum (Fig. 6b).

Coordination polymers with d^{10} metal centers are of great interest owing to their potential applications in chemical sensors and photochemistry, but researches concerning silver luminescent compounds are limited. The solid-state photoluminescent properties of the free ligands and complexes **I** and **II** have been investigated in the solid state at room temperature, as shown in Fig. 7. The emission peak of free Bpp ligand is observed at about 440 nm (under excitation at 348 nm) resulting from the π–π* or *n*–π* transitions [49], whereas the Dcia ligand shows almost no contribution to the emissions of the compounds due to its very weak fluorescent emission. On complexation of Bpp ligand with Ag(I) atom, complex **I** exhibits maximum emission band observed at 375 nm under excitation at 260 nm. In contrast to the emission of the free Bpp ligand, complex **I** shows blue-shift of ~65 nm, which may be assigned to the ligand-to-metal charge transfer (LMCT) from the Bpp ligand to the Ag(I) ions [50]. However, the emission peak for complex **II** occurs at about 401 nm under excitation at 323 nm with blue-shift of ~39 nm with respect to the emission shown by the Bpp ligand. They can probably be assigned to the

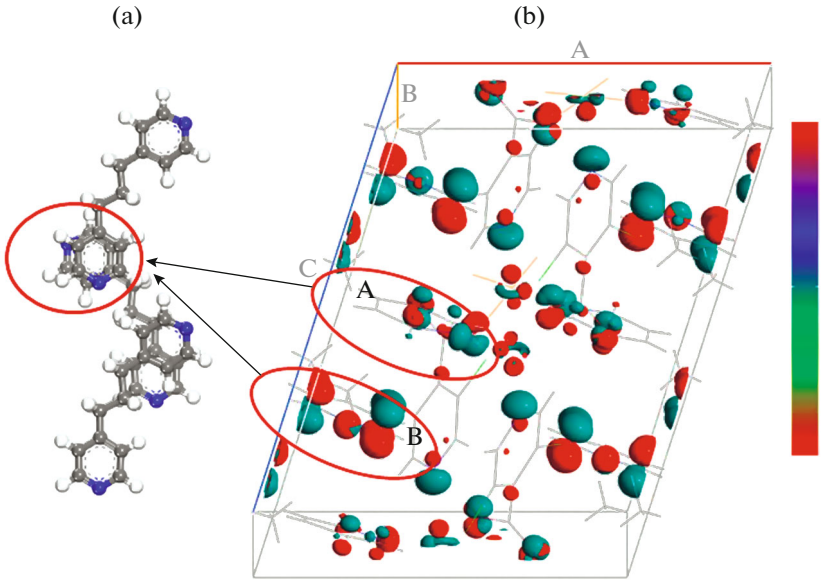

Fig. 4. Local structure of pyridine rings in complex **II** (a); crystal structure and valence electron density (b). (The color represents a phase of Bloch state. A with red circle Stands for pyridine rings in Bpp molecule and B with red circle stands for another pyridine rings.)

intraligand charge transfer of Bpp ligand, whereas the blue-shift may be attributed to the coordination effects of the Bpp ligands to Cd(II) cations, which increases the ligand conformational rigidityit and reduces the nonradiative decay of the intraligand [51, 52]. Although more detailed theoretical and spectroscopic studies may be necessary for better understanding of the luminescent mechanism, the fluorescence emission of both complexes make it potentially useful photoactive material.

In summary, two novel Ag(I)/Cd(II) coordination polymers with different structure motifs have been synthesized by the hydrothermal reaction. Although two complexes are contrasted by the same ligands, the structure of them reveal entirely different 2D networks: the 2D cationic layer with 3-connected $\{6^3\}$ *hcb* topology of **I** is developed by T-shaped Bpp-bridging Ag–Ag building units, whereas complex **II** shows Dcia-bridged grid layer joined by the right-handed and left-handed helical chains. The luminescent properties of **I** and **II** indicate that the coordination of metal ion can affect the emission peak of the organic material. Further studies and physical characterizations of other transition metals with the HDcia ligand are also underway in our lab.

FUNDING

This work was supported by the National Natural Science Foundation of China (grant no. 21571093).

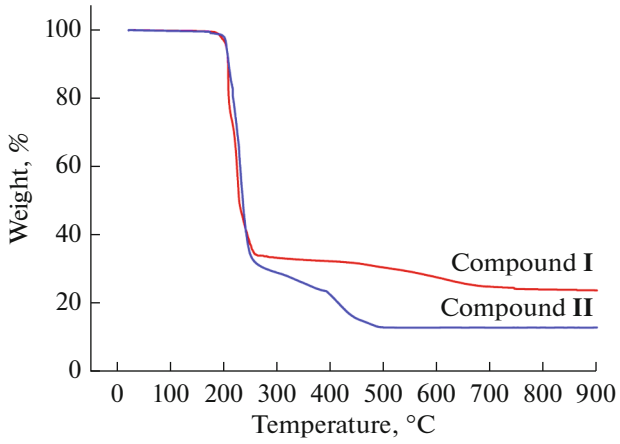

Fig. 5. TGA curve for compound **I** (a) and **II** (b).

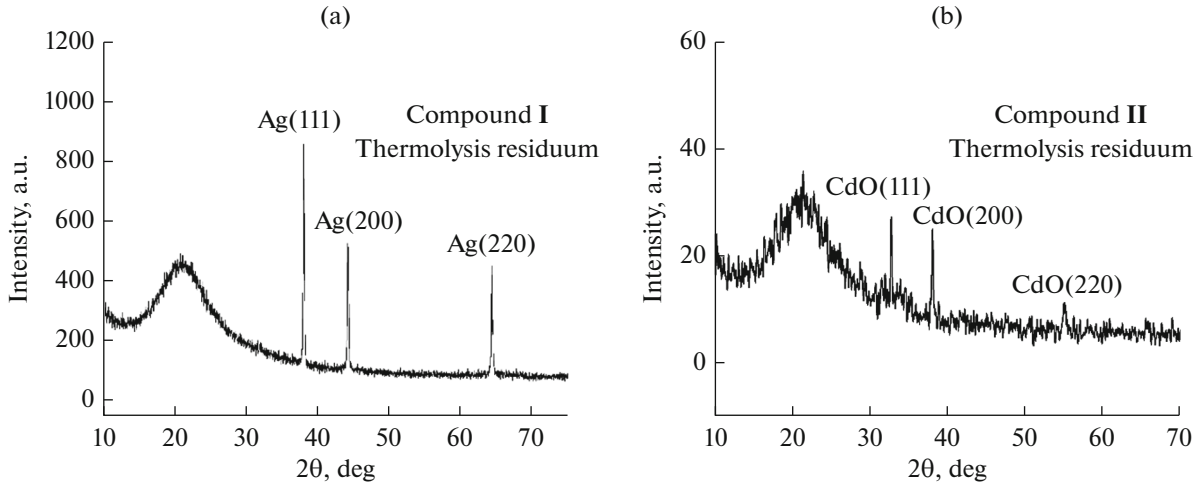

Fig. 6. The PXRD patterns of thermolysis residuum for compounds **I** (a) and **II** (b).

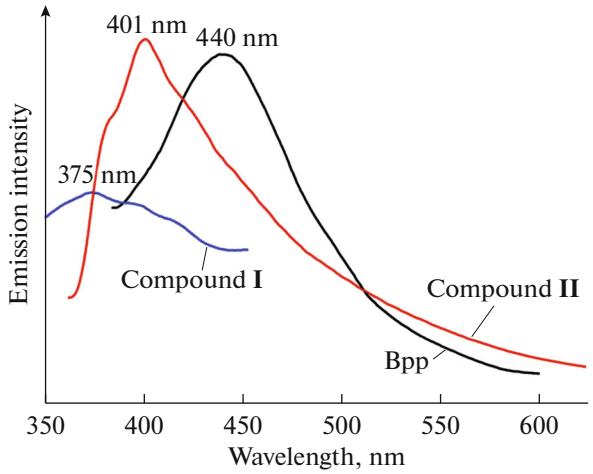

Fig. 7. Solid-state emission spectra of compounds **I**, **II** and the free Bpp ligand at ambient temperature.

CONFLICT OF INTEREST

The authors declare that they have no conflicts of interest.

REFERENCES

1. Yang, X.G., Ma, L.F., and Yan, D.P., *Chem. Sci.*, 2019, vol. 10, no. 17, p. 4567.
2. Wang, X.D. and Wolfbeis, O.S., *Chem. Soc. Rev.*, 2014, vol. 43, p. 3666.
3. Ramaswamy, P., Wong, O.E., Gelfand, B.S., and Shimizu, G.K.H., *J. Am. Chem. Soc.*, 2015, vol. 137, p. 7640.
4. Shi, D., Zheng, R., Sun, M.J., et al., *Angew. Chem. Int. Ed.*, 2017, vol. 56, p. 14637.
5. Kurmoo, M., *Chem. Soc. Rev.*, 2009, vol. 38, p. 1353.
6. Li, X.L., Liu, G.Z., Xin, L.Y., and Wang, L.-Y., *J. Solid State Chem.*, 2017, vol. 246, p. 252.
7. Zhao, Y., Deng, D.S., Ma, L.F., et al., *Chem. Commun.*, 2013, vol. 49, p. 10299.
8. Xue, L.P., Li, Z.H., Zhang, T., et al., *New J. Chem.*, 2018, vol. 42, p. 14203.
9. Lian, X. and Yan, B., *Inorg. Chem.*, 2017, vol. 56, p. 6802.
10. Li, J.X. and Du, Z.X., *J. Clust. Sci.*, 2020, vol. 31, p. 507.
11. Xin, L.Y., Liu, G.Z., Li, X.L., and Wang, L.Y., *Cryst. Growth Des.*, 2012, vol. 12, p. 147.
12. Wang, Y.F., Li, M.H., and Wang, L.Y., *Russ. J. Gen. Chem.*, 2020, vol. 90, no. 2, p. 305. https://doi.org/10.1134/S1070363220020231
13. Xin, L.Y., Li, X.L., Yin, W.D., and Liu, G.Z., *Chin. J. Struct. Chem.*, 2020, vol. 39, no. 5, p. 933.
14. Li, N., Zhu, Q.E., Hu, H.M., et al., *Polyhedron*, 2013, vol. 49, p. 207.
15. Wang, J., Wu, X.R., Liu, J.Q., et al., *J. Clust. Sci.*, 2015, vol. 26, p. 827.

16. Chen, J. and Kitagawa, S., *Chem. Lett.*, 2011, vol. 40, no. 6, p. 656.
17. Wang, Y.F., Tai, J.H., Yan, X.W., et al., *Chin. J. Inorg. Chem.*, 2018, vol. 34, p. 1121.
18. Yokoi, T., Goto, T., Hara, M., et al., *Chem. Commun.*, 2021, vol. 4, p. 4.
19. Wang, Y.F., Li, Z., Sun, Y.C., et al., *Inorg. Chem. Commun.*, 2014, vol. 44, p. 25.
20. Ju, F.Y. and Li, S., *Russ. J. Gen. Chem.*, 2020, vol. 90, p. 1083. https://doi.org/10.1134/S1070363220060237
21. Liu, G.Z., Li, S.H., Li, X.L., et al., *CrystEngComm*, 2013, vol. 15, p. 4571.
22. Lei, M.Y., Wang, X.H., Shi, Y., and Zhang, Q.F., *J. Clust. Sci.*, 2020, vol. 31, no. 2, p. 347.
23. Xue, L.P. and Ding, K.X., *Chin. J. Struct. Chem.*, 2020, vol. 39, no. 7, p. 1295.
24. Li, G.L., Yin, W.D., Liu, Q.L., et al., *Chin. J. Inorg. Chem.*, 2019, vol. 35, p. 2355.
25. Hu, F.L., Shi, Y.X., Chen, H.H., and Lang, J.P., *Dalton Trans.*, 2015, vol. 44, p. 18795.
26. Xue, L.P. and Zhang, Y.G., *J. Sulfur. Chem.*, 2020, vol. 41, no. 3, p. 293.
27. Xin, L.Y., Liu, G.Z., Ma, L.F., and Wang, L.Y., *J. Solid State Chem.*, 2013, vol. 206, p. 233.
28. Li, Y.P., Ju, F.Y., Li, G.L., et al., *Russ. J. Coord. Chem.*, 2018, vol. 44, p. 214. https://doi.org/10.1134/S1070328418030028
29. Zhou, L., Zhou, B.L., Cui, Z., et al., *CrystEngComm*, 2018, vol. 20, p. 5402.
30. Siddiqui, K.A. and Lama, P., *J. Struct. Chem.*, 2018, vol. 59, no. 1, p. 166.
31. Zhou, L., Fan, H.H., Zhou, B.L., et al., *Dalton Trans.*, 2019, vol. 48, p. 296.
32. Mei, L., Wang, C.Z., Wang, L., et al., *Cryst. Growth Des.*, 2015, vol. 15, p. 1395.
33. Mei, L., Hu, K.Q., Zhang, Z.H., et al., *Inorg. Chem.*, 2018, vol. 57, p. 4673.
34. Xin, L.Y.., Ji, Z.R., and Guo, R.R., *Z. Kristallogr. – New Cryst. Struct.*, 2019, vol. 234, no. 3, p. 495.
35. Li, X.L., Feng, K.X., and Xin, L.Y., *Z. Kristallogr. – New Cryst. Struct.*, 2019, vol. 234, no. 4, p. 639.
36. Sun, X.T. and Zheng, L., *Z. Kristallogr. – New Cryst. Struct.*, 2020, vol. 235, no. 4, p. 793.
37. Dolomanov, O.V., Bourhis, L.J., Gildea, R.J., et al., *J. Appl. Cryst.*, 2009, vol. 42, p. 339.
38. Sheldrick, G.M., *Acta Crystallogr., Sect. A: Found. Adv.*, 2015, vol. 71, p. 3.
39. Sheldrick, G.M., *Acta Crystallogr., Sect. C: Struct. Chem.*, 2015, vol. 71, p. 3.
40. Chiang, L.M., Yeh, C.W., Chan, Z.K., et al., *Cryst. Growth Des.*, 2008, vol. 8, no. 2, p. 470.
41. Yaghi, O.M. and Li, H.L., *J. Am. Chem. Soc.*, 1996, vol. 118, p. 295.
42. Dai, L.M., You, W.S., Wang, E.B., et al., *Cryst. Growth Des.*, 2009, vol. 9, p. 2110.
43. Li, Z.H., Li, Z.Y., Chen, Y., et al., *Chin. J. Struct. Chem.*, 2018, vol. 37, no. 4, p. 617.
44. Xin, L.Y., Li, Y.P., Ju, F.Y., et al., *Chin. J. Inorg. Chem.*, 2017, vol. 33, no. 8, p. 1474.
45. Brandbyge, M., *Phys. Rev. B: Condens. Matter Mater. Phys.*, 2002, vol. 65, no. 16, p. 5401.
46. Soler, J.M., Artacho, E., Gale, J.D., et al., *J. Phys. Condens. Matt.*, 2002, vol. 14, no. 11, p. 2745.
47. Perdew, J.P., Burke, K., and Ernzerhof, M., *Phys. Rev. Lett.*, 1996, vol. 77, no. 18, p. 3865.
48. Shin, H., Kim, J., Lee, H., et al., *J. Chem. Theor. Comput.*, 2017, vol. 13, no. 11, p. 5639.
49. Qin, T., Zhang, S.L., Wang, Y.X., et al., *Acta Crystallogr., Sect. C: Struct. Chem.,* 2019, vol. 75, p. 150.
50. Shen, S.S., Wang, X.F., Hu, H.M., et al., *Polyhedron*, 2015, vol. 91, p. 152.
51. Bai, H.Y., Ma, J.F., Yang, J., et al., *Cryst. Growth Des.*, 2010, vol. 10, no. 4, p. 1946.
52. He, Y.C., Yuan, Z.H., Zhang, J., et al., *Inorg. Chim. Acta.*, 2020, vol. 511, p. 119802.